Evidence for liquid water during the high-density to low-density amorphous ice transition

Chae Un Kim[a], Buz Barstow[b], Mark W. Tate[c,d], and Sol M. Gruner[a,c,d,1]

[a]Cornell High Energy Synchrotron Source, [b]School of Applied Physics, [c]Laboratory of Atomic and Solid-State Physics, and [d]Department of Physics, Cornell University, Ithaca, NY 14853

Polymorphism of water has been extensively studied, but controversy still exists over the phase transition between high-density amorphous (HDA) and low-density amorphous (LDA) ice. We report the phase behavior of HDA ice inside high-pressure cryocooled protein crystals. Using X-ray diffraction, we demonstrate that the intermediate states in the temperature range from 80 to 170 K can be reconstructed as a linear combination of HDA and LDA ice, suggesting a first-order transition. We found evidence for a liquid state of water during the ice transition based on the protein crystallographic data. These observations open the possibility that the HDA ice induced by high-pressure cryocooling is a genuine glassy form of high-density liquid.

liquid–liquid hypothesis | supercooled water | water phases | high-density liquid

Supercooled water shows anomalous thermodynamic behavior (1–3). Theories that account for these anomalous properties include the stability limit (4), the singularity-free (5, 6), and the liquid–liquid (LL) critical point (7) hypotheses. The latter 2 hypotheses propose the existence of 2 distinct forms of supercooled water: high-density liquid (HDL) and low-density liquid (LDL) water (8). In the singularity-free hypothesis, HDL transforms continuously to LDL. In the LL critical point theory, HDL undergoes a first-order phase transition to LDL (8). However, experimental study of the HDL–LDL phase transition is challenging as supercooled water spontaneously converts to crystalline forms below the homogeneous nucleation temperature ($\approx$235 K at 0.1 MPa). The transition between 2 glassy forms of water, high-density amorphous (HDA) and low-density amorphous (LDA) ice, has been extensively studied (9–18), as an analogue of the HDL–LDL transition. Controversy still exists as to whether the HDA–LDA ice transition is truly a first-order phase transition (10–13) or if it occurs because of a relaxation process of an unstable amorphous structure (15–18). More importantly, the connection between the HDA–LDA ice transition and the HDL–LDL phase transition, implied by thermodynamic and structural studies on water (19–22), remains challenging to prove experimentally (8).

We used X-ray diffraction to study the transition of HDA to LDA ice in protein crystals. HDA ice was induced inside protein crystals by a high-pressure cryocooling method (23) originally developed for macromolecular crystallography (23–26). The Bragg diffraction from protein crystals mainly provides information on protein structure. The simultaneously recorded water diffuse diffraction (WDD) profile reports on the phase of the water in the protein crystal, which accounts for typically 40–60% of its volume.

Results

Fig. 1 shows diffraction images and the WDD profiles from a high-pressure cryocooled crystal of the globular protein thaumatin. As the crystal temperature is increased from 80 to 170 K, the primary WDD peak, corresponding to the mean distance between neighboring water molecule oxygen atoms, shifts to lower momentum transfer (Q) region [$Q = 4\pi\sin(\theta)/\lambda$, where λ

is the X-ray wavelength and 2θ is the angle between the incident and diffracted X-ray beams] (Fig. 1A), indicating a phase transition from HDA to LDA ice (27). As the crystal temperature is increased, the superimposed WDD profiles (Fig. 1B) exhibit isosbestic points, as expected for a first-order phase transition. A singular value decomposition (SVD) analysis (Fig. 1C) demonstrates that the WDD profiles between 80 and 170 K can be reconstructed as a linear combination of the high-density state at 80 K and the low-density state at 170 K. The WDD profile in the transition region between 80 and 170 K is consistent with a monotonically decreasing HDA phase and a monotonically increasing LDA phase, as shown in Fig. 1D. This 2-state reconstruction is strong evidence that the HDA ice induced inside the protein crystal undergoes a first-order phase transition to LDA ice.

The unit-cell volume of a thaumatin crystal, high-pressure cryocooled at 200 MPa, warmed from 80 to 170 K is shown in Fig. 2A. The primary WDD peak position is plotted as an indicator for the HDA to LDA ice phase transition. The small increase of the crystal unit-cell volume between 80 and 170 K is inconsistent with ice expansion during the HDA to LDA phase transition. Assuming that the unit cell retains all water, and a water volume expansion of $\approx$24% during the HDA to LDA ice phase transition (9), the unit cell ($\approx$60% water by volume) should expand by $\approx$14%. Even if we assume that the water in the protein hydration layer ($\approx$15%) does not undergo the ice phase transition, the unit cell should still expand by $\approx$11%. However, the observed total unit-cell volume expansion from 80 to 170 K is only $\approx$5%. As the observed unit-cell expansion is partially caused by thermal expansion of the protein and radiation damage (28), the contribution of water during the ice phase transition to the unit-cell expansion becomes even smaller. A possible explanation for this discrepancy is that the solvent water flows from the unit cell of the crystal to adjacent inclusions or to the crystal surface during the HDA to LDA phase transition. This idea suggests that the water, rather than remaining continuously in solid amorphous states, exists in a liquid state during the phase transition. As a control, the crystal unit-cell volume of an ambient-pressure cryocooled thaumatin crystal was measured as under warming (Fig. 2B). In this case, the LDA ice formed inside the crystal during cryocooling remains in the LDA state under warming up to 165 K. The primary WDD peak position does not change appreciably and the unit-cell volume expansion between 80 and 165 K is $\approx$1%, which we ascribe to thermal expansion of the protein and radiation damage.

Crystal mosaicity (Fig. 2A), a measure of orientational order between unit cells, was monitored to probe rearrangement of the thaumatin molecules in the high-pressure cryocooled crystal
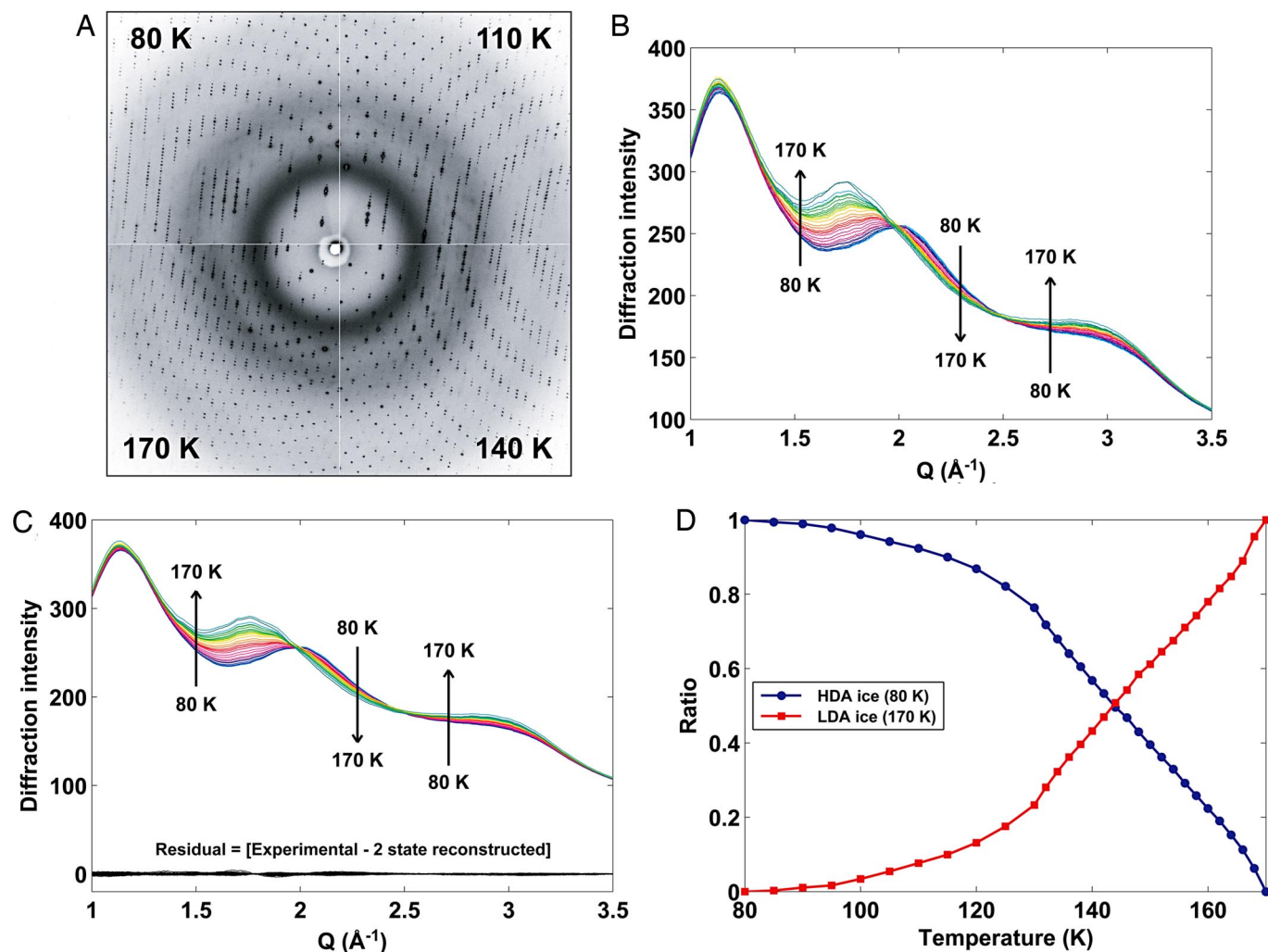
Fig. 1. Thaumatin diffraction of a crystal high-pressure cryocooled at 200 MPa. (*A*) Bragg and diffuse diffraction shown at 80, 110, 140, and 170 K. The primary WDD peak (second innermost ring) at Q = 2.03 Å^{-1} indicates HDA ice at 80 K and shifts to 2.00 Å^{-1} at 110 K, 1.92 Å^{-1} at 140 K, and finally to 1.73 Å^{-1}, indicative of LDA ice at 170 K. The inner diffuse ring (Q = 1.2 Å^{-1}) is from an oil coating applied to the crystal. (*B*) Radially integrated WDD profiles from crystal diffraction images. The 31 superimposed WDD profiles from 80 to 170 K show isosbestic points at Q = 2.0 and 2.5 Å^{-1}. (*C*) WDD profiles reconstructed from 2 states via SVD analysis. Residuals were calculated by subtracting the reconstructed profile from the experimental WDD profile at each temperature. (*D*) Ratio of HDA ice at 80 K and LDA ice at 170 K used to reconstruct the transition WDD states between 80 and 170 K in the SVD analysis.

under warming. The crystal mosaicity drops by ≈25% between 135 and 145 K, indicating improved ordering of the proteins during the water phase transition. This unexpected crystal "self-healing" effect suggests that the protein molecules were able to rearrange to improve the molecular packing, as if they were in a liquid environment as in the conventional macromo- lecular crystal annealing (29–31). As shown in Fig. 2*B*, the crystal self-healing effect is not observed in the ambient-pressure cryocooled thaumatin crystal, confirming that the molecular rearrangement requires the water phase transition.

The effects of the water phase transition on the atomic structure of the protein were investigated by collecting 13 complete diffraction datasets between 80 and 165 K from a single high-pressure cryocooled thaumatin crystal. Fig. 3*A* shows the superimposed solvent channels of the crystal along the crystallographic *a*-axis at 80 and 165 K. The protein structure changes little under warming, and the negligible size increase of the solvent channel between 80 and 165 K is too small to accommodate the ≈24% water expansion during the HDA to LDA phase transition. For the water to expand isotropically and remain within the solvent channels, an estimated 7% increase in

channel radius would be required. Fig. 3*B* shows a disulfide bond between cysteine amino acid residues, Cys-159 and Cys-164, of the high-pressure cryocooled thaumatin upon warming. It is observed that at <100 K only one rotamer conformation is dominant. Upon warming to 160 K, the electron density of a second conformation gradually emerges. As shown in Fig. 3*C*, the secondary disulfide rotamer conformation is always present in the ambient-pressure structures over the entire temperature range from 80 to 293 K. The observation in Fig. 3*B* implies that the first rotamer conformation was favored by high-pressure cryocooling and, upon warming, relaxed to the 2-conformation state preferred at ambient pressure. This site-specific, anhar- monic structural relaxation between 100 and 160 K suggests a flexible environment around the protein molecule during the ice phase transition.

Structural relaxation over the whole molecule was monitored via the atomic temperature Debye-Waller factor (*B* factor) during the ice phase transition. In macromolecular crystallog- raphy, the *B* factors represent the effects of conformational fluctuations and static lattice disorder of the molecule (32, 33). Fig. 4*A* shows the *B*-factor values along the main chain of the
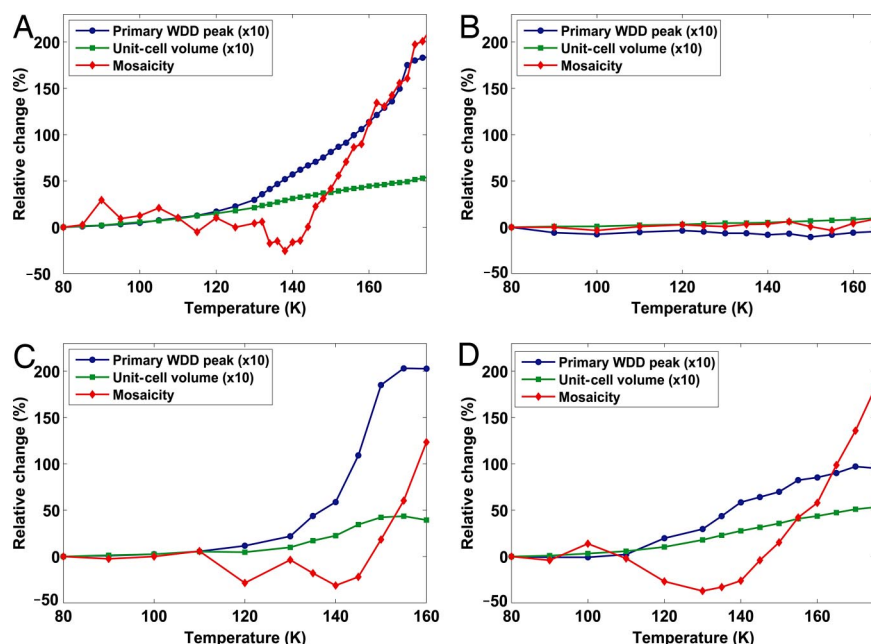
Fig. 2. Parameters from protein crystals warmed from 80 to 170 K. (*A* and *B*) Thaumatin crystal high-pressure cryocooled at 200 MPa (*A*) and cryocooled at ambient pressure (0.1 MPa) (*B*). (*C* and *D*) Glucose isomerase crystal high-pressure cryocooled at 180 MPa (*C*) and elastase crystal high-pressure cryocooled at 200 MPa (*D*). Relative changes of the primary WDD peak position (blue, circle) in *d*-spacing (*d* = 2 π/Q), crystal unit-cell volume (green, square), and crystal mosaicity (red, diamond) are shown. The values for WDD peak position and unit-cell volume are multiplied by 10.

high-pressure cryocooled thaumatin molecule from 80 to 165 K. The *B*-factor profile from a thaumatin molecule at ambient conditions (i.e., 0.1 MPa and 293 K) is plotted for reference. The *B*-factor profile begins to rise at ≈135 K. By 165 K the *B*-factor profile resembles that at ambient conditions. Under cooling from room temperature to cryogenic temperatures, the collective thermal motions of the protein molecule are damped and static disorder becomes dominant. Fig. 4*A* suggests that the thermal motions of the protein molecule that were damped by high-pressure cryocooling have been released during crystal warming. This result supports the conclusion that the thaumatin molecules were exposed to a flexible environment during the temperature increase from 80 to 165 K. As a control, the *B* factors from an ambient-pressure cryocooled thaumatin crystal are plotted from 80 to 165 K (Fig. 4*B*). The *B*-factor profiles over the entire temperature range show no significant rise and exhibit a distinct difference from the profile at ambient conditions. This result indicates that the damped thermal motion of the protein is not released over this temperature range if the molecule is trapped in the LDA ice state. Hence, the *B*-factor increase in Fig. 4*A* is directly related to the state of water during the phase transition and is not a consequence of the temperature rise alone.

The unit-cell volume increase shown in Fig. 2*A* is reproducible in other thaumatin crystals (Fig. S1). Furthermore, these observations are not specific to thaumatin because evidence for fluid water is also observed in glucose isomerase and elastase crystals (Fig. 2 *C* and *D*, respectively). In both cases, the phase transition from HDA to LDA ice begins at ≈100 K. As with thaumatin, the unit-cell volume expansion during the HDA to LDA phase transition is too small to accommodate the expanded water. Crystal self-healing is also observed during the ice phase transition in these crystals. The 3 types of protein crystals used in this study have differing crystallization conditions, crystal symmetries, solvent channel networks, and total water contents. Nonetheless, they all display behavior under warming that suggests the existence of liquid water at temperatures ranging from 80 to 170 K. Therefore, we believe that our results reflect the intrinsic

properties of water confined within the macromolecular channels inside the high-pressure cryocooled protein crystals.

Discussion

It has been reported that the HDA ice prepared by the conventional method [compressing hexagonal ice >1 GPa at 77 K (9)] exhibits a relaxation process in the transition to LDA ice (15–18). Using high-pressure cryocooling, HDA ice is induced by pressurizing samples at 283 K, which are then cooled to 77 K while still under pressure (23). As shown in this study, the HDA ice induced by high-pressure cryocooling leads to a first-order phase transition to LDA ice even without annealing at high pressure (13). More importantly, our observations provide evidence for a liquid state of water during the ice transition, suggesting a possible glass transition of HDA ice, which opens the possibility that the HDA ice induced by high-pressure cryocooling may be a true glassy form of HDL.

It has been proposed that HDA ice is thermodynamically smoothly connected to HDL water (19–21) and that LDA ice is structurally related to LDL water (8, 34–36). Combined with the evidence for liquid water in this study, these predictions suggest that both HDL and LDL water may coexist during the ice phase transition inside high-pressure cryocooled protein crystals. If so, it is plausible that the observed first-order phase transition is a transition between HDL and LDL water. This interpretation is supported by the LL critical point theory, which predicts a first-order transition from HDL to LDL water (7). These predictions and the experimental results presented here suggest that during warming of high-pressure cryocooled protein crystals, HDA ice first transforms smoothly to HDL water, then undergoes a first-order transition to LDL water, and finally continuously converts to LDA ice.

Further work is needed to provide more direct evidence on the existence of liquid water and resolve subtleties in the liquid states (i.e., HDL and LDL). It also remains to be seen whether the liquid state of water exists during the HDA to LDA ice transition not only in the water confined to the interior spaces of a protein crystal but also in high-pressure cryocooled bulk water (27).
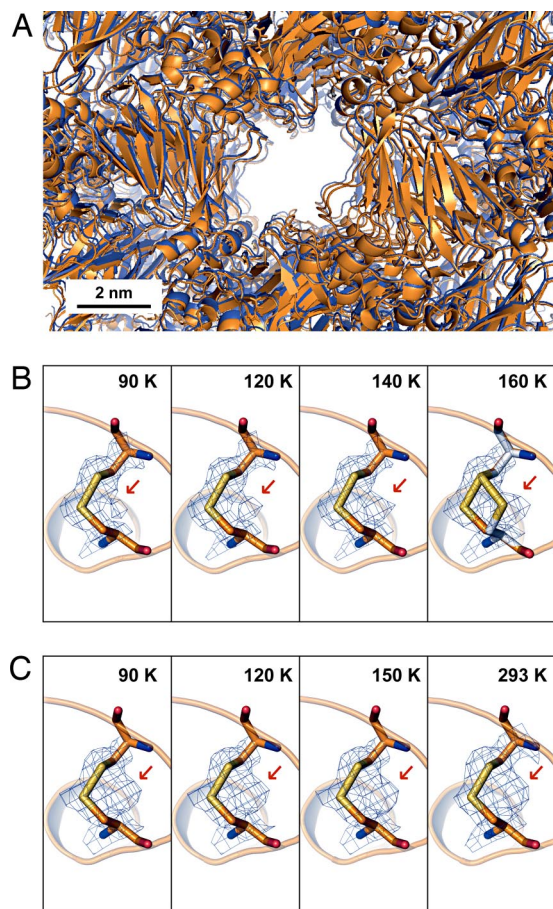
Fig. 3. Crystal solvent channel and site-specific relaxation of thaumatin molecule. (*A*) Solvent channels superimposed along the *a*-axis of a thaumatin crystal high-pressure cryocooled at 200 MPa. Blue represents atomic packing at 80 K, where HDA ice is metastable. Orange represents atomic packing at 165 K, where the phase transition to LDA ice is almost complete. Size variation of the solvent channels is negligible. (*B*) Disulfide bond between Cys-159 and Cys-164 of the high-pressure cryocooled thaumatin upon warming (F_o electron density map, 1-σ level). Red arrow indicates electron density for the secondary rotamer conformation. The refined disulfide bond model for the second conformation is present in the electron density at 160 K. (*C*) Disulfide bond between Cys-159 and Cys-164 of thaumatin at ambient pressure. The disulfide bond model refined into the second conformation electron density (red arrow) is not shown to clarify the electron density.

Experiments with faster time resolution (37) and that directly probe the dynamic properties of liquid water (38, 39) may provide more insight into the phase behavior of supercooled water.

Materials and Methods

Protein Crystallization. Lyophilized thaumatin powder from *Thaumatococcus daniell* (catalog no. T7638; Sigma) was used for crystallization without further purification. Crystals were grown at 20 °C by the hanging-drop method with 25 mg/mL thaumatin solution in 50 mM Hepes buffer at pH 7 and crystallization solution containing 0.9 M sodium potassium tartrate as a precipitant (27). The crystal space group was determined to be P4$_1$2$_1$2, having a solvent content of 60% by volume.

Glucose isomerase from *Streptomyces rubiginosus* was purchased from Hampton Research (catalog No. HR7-102). Crystals were grown by the hanging-drop method by mixing a reservoir solution containing 1.15 M ammonium sulfate, 1 mM magnesium sulfate, and 10 mM Hepes, pH 7.5, with 25 mg/mL protein solution in pure water (27). The crystal space group was determined to be I222, having a solvent content of ≈55%.

Lyophilized porcine pancreas elastase (catalog no. 20929; SERVA) was used for crystallization without further purification. Crystals were grown by the
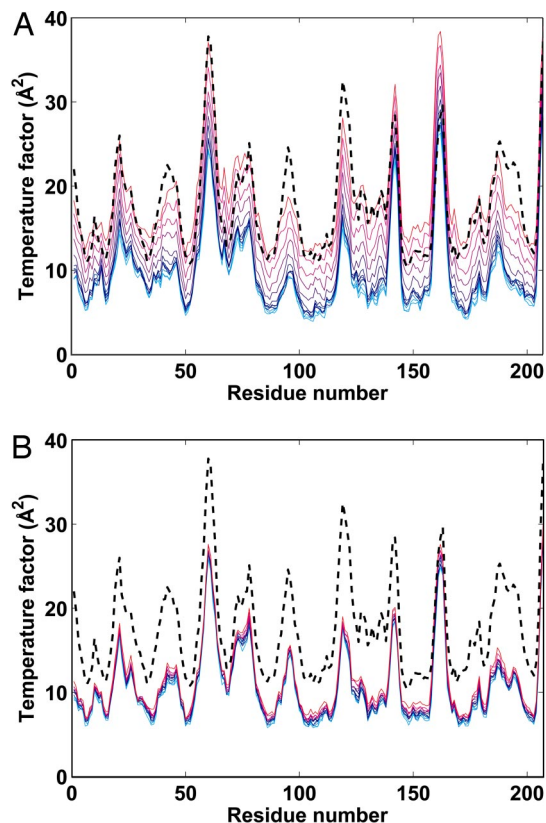

Fig. 4. Thaumatin *B* factors to probe for molecular relaxation. (*A*) *B*-factor profiles of thaumatin high-pressure cryocooled at 200 MPa along its main chain are shown. Each profile is 1 of 13 profiles from 80 to 165 K (blue = low temperatures and red = high temperatures). The *B*-factor profile from thaumatin at ambient conditions (0.1 MPa and 293 K) is superimposed as a reference (dotted black line). (*B*) *B*-factor profiles of thaumatin cryocooled at ambient pressure (0.1 MPa) are shown. Each profile is 1 of 13 profiles from 80 to 165 K (blue = low temperatures and red = high temperatures). The dotted black line is the profile at ambient conditions.

hanging-drop method by mixing a reservoir solution containing 30 mM sodium sulfate and 50 mM sodium acetate, pH 5.0 with a 25 mg/mL protein solution in pure water (27). The crystal space group was determined to be P2$_1$2$_1$2$_1$, having a solvent content of ≈40%.

Crystal Cryocooling. High-pressure cryocooling of crystal samples was carried out as described by Kim et al. (23). In brief, samples were loaded into the high-pressure cryocooling apparatus, which was then pressurized with helium gas to 200 MPa at ambient temperature. Once at high pressure, the samples were dropped into a zone that was precooled to liquid-nitrogen temperature (77 K). Helium pressure was then released. Thereafter crystal samples were handled/stored at ambient pressure and at liquid-nitrogen temperature before X-ray diffraction measurements.

For the crystal cryocooling at ambient pressure, 25% glycerol was added to crystals as a cryoprotectant to prevent the crystalline ice formation. Then the crystal was cryocooled by directly plunging into liquid nitrogen at ambient pressure.

X-Ray Diffraction Data Collection. The X-ray diffraction data were collected at the macromolecular crystallography stations A1 ($\lambda = 0.9771$ Å, ADSC Quantum 210 CCD detector, beam size of 100 μm), F1 ($\lambda = 0.9179$ Å, ADSC Quantum 270 CCD detector, beam size of 100 μm), and F2 ($\lambda = 0.9795$ Å, ADSC Quantum 210 CCD detector, beam size of 150 μm) at the Cornell High Energy Synchrotron Source. The high-pressure cryocooled crystals were carefully transferred from liquid nitrogen to a goniometer to prevent sample warming. During data collection, the sample temperature ranging from 80 to 170 K was controlled by a Cryostream 700 series cryocooler from Oxford Cryosystems. During the warming studies, sample temperature was increased at the rate of 2–6 K/min. After reaching a desired temperature, samples were left at the temperature

for 5–10 min for equilibration. The X-ray diffraction data of the protein crystals were collected with temperature steps of 2 or 5 to 10 K, with the smaller temperature steps taken in the vicinity of the phase transition.

For the crystal diffraction data analysis in Fig. 2, 5 consecutive images were collected at each temperature, with an oscillation angle of 1° starting at the same crystal orientation. The X-ray exposure time was 3–5 s. The momentum transfer vector Q is given by $Q = 4\,\pi\sin(\theta)/\lambda$, where λ is the X-ray wavelength and 2θ is the angle between the incident beam and the diffracted X-rays. The corresponding d-spacing in real space is given by $d = 2\pi/Q$.

To study the solvent channels and the atomic temperature factors of thaumatin, shown in Figs. 3 and 4, 13 complete diffraction datasets (each of 60 frames with 1° oscillation) were collected between 80 and 165 K with the 5–10 K temperature increment from a single thaumatin crystal high-pressure cryocooled at 200 MPa. Another 13 complete datasets from a single thaumatin crystal cryocooled at ambient pressure were collected as a control. Finally, a complete dataset from an unfrozen thaumatin crystal at ambient conditions [ambient pressure (0.1 MPa), 293 K] was collected as a reference. Details on the data collection statistics can be found in Tables S1 and S2.

Data Analysis. *Diffuse diffraction from water.* Each diffraction pattern from a protein crystal consists of Bragg peaks from the protein molecules in the crystal superimposed on the diffuse diffraction rings arising from the oil external to the crystal and water internal to the crystal. The underlying diffuse diffraction was isolated from the Bragg spots by applying a custom polar-coordinate median filter to the intensity values of the image (27). The sample-to-detector distance was calibrated based on the known Bragg peaks of hexagonal ice. Peak positions for the WDD were determined by fitting a quadratic function in the vicinity of the maxima.

Crystal diffraction. Unit-cell parameters and crystal mosaicity at each temperature in Fig. 2 were refined by processing 5 consecutive 1° oscillation images with DPS (40) and HKL2000 (41), independently. Fig. S2 shows the result of data analysis with DPS and HKL 2000 for comparison. Both programs yielded the same trends of unit-cell volume and mosaicity as a function of temperature, with only minor differences, implying that the results are not artefacts of the data analysis programs.

The complete 13 datasets from a high-pressure cryocooled thaumatin crystal at 200 MPa described in the data collection section could also generate the unit-cell and mosaicity profiles as a function of temperature as in Fig. S1. This finding confirms that the trend in Fig. 2A is reproducible in other thaumatin crystals.

Structure Refinement. The complete thaumatin datasets used for Figs. 3 and 4 were indexed, prerefined, integrated, postrefined, scaled, and merged with HKL2000 (41). The initial structures were determined by the molecular-replacement method using MOLREP (42) from the CCP4 program suite (43). The structures were then refined against the dataset with REFMAC5 (44). The refined structures were proofread with COOT (45). The refined structures in Fig. 3 were generated with PYMOL (46). Details on the refinement statistics can be found in Table S3.

1. Angell CA (1982) in *Water: A Comprehensive Treatise*, ed Franks F (Plenum, New York), Vol 7, pp 1–81.
2. Debenedetti PG, Stanley HE (2003) Supercooled and glassy water. *Phys Today* 56:40–46.
3. Debenedetti PG (2003) Supercooled and glassy water. *J Phys Condens Matter* 15:R1669–R1726.
4. Speedy RJ (1982) Stability-limit conjecture. An interpretation of the properties of water. *J Phys Chem* 86:982–991.
5. Stanley HE, Teixeira J (1980) Interpretation of the unusual behavior of H_2O and D_2O at low temperatures: Tests of a percolation model. *J Chem Phys* 73:3404–3422.
6. Sastry S, Debenedetti P, Sciortino F, Stanley HE (1996) Singularity-free interpretation of the thermodynamics of supercooled water. *Phys Rev E* 53:6144–6154.
7. Poole PH, Sciortino F, Essmann U, Stanley HE (1992) Phase behavior of metastable water. *Nature* 360:324–328.
8. Mishima O, Stanley HE (1998) The relationship between liquid, supercooled, and glassy water. *Nature* 396:329–335.
9. Mishima O, Calvert LD, Whalley E (1984) ''Melting'' ice I at 77 K and 10 kbar: A new method of making amorphous solids. *Nature* 310:393–395.
10. Mishima O, Calvert LD, Whalley E (1985) An apparently first-order transition between two amorphous phases of ice induced by pressure. *Nature* 314:76–78.
11. Mishima O, Suzuki Y (2002) Propagation of the polyamorphic transition of ice and the liquid–liquid critical point. *Nature* 419:599–603.
12. Koltz S, et al. (2005) Nature of the polyamorphic transition in ice under pressure. *Phys Rev Lett* 94:025506.
13. Nelmes RJ, et al. (2006) Annealed high-density amorphous ice under pressure. *Nature Phys* 2:414–418.
14. Mishima O, Suzuki Y (2001) Vitrification of emulsified liquid water under pressure. *J Chem Phys* 115:4199–4202.
15. Tulk CA, et al. (2002) Structural studies of several distinct metastable forms of amorphous ice. *Science* 297:1320–1323.
16. Guthrie M, et al. (2003) Direct structural measurements of relaxation processes during transformations in amorphous ice. *Phys Rev B* 68:184110.
17. Tse JS, et al. (2005) Investigation of the intermediate- and high-density forms of amorphous ice by molecular dynamics calculations and diffraction experiments. *Phys Rev B* 71:214107.
18. Koza MM, May RP, Schober H (2007) On the heterogeneous character of water's amorphous polymorphism. *J Appl Crystallogr* 40:S517–S521.
19. Whalley E, Klug DD, Handa YP (1989) Entropy of amorphous ice. *Nature* 342:782–783.
20. Johari GP, Fleissner G, Hallbrucker A, Mayer E (1994) Thermodynamic continuity between glassy and normal water. *J Phys Chem* 98:4719–4725.
21. Speedy RJ, Debenedetti PG, Smith RS, Huang C, Kay BD (1996) The evaporation rate, free energy, and entropy of amorphous water at 150 K. *J Chem Phys* 105:240–244.
22. Finney JL, Hallbrucker A, Kohl I, Soper AK, Bowron DT (2002) Structures of high- and low-density amorphous ice by neutron diffraction. *Phys Rev Lett* 88:225503.
23. Kim CU, Kapfer R, Gruner SM (2005) High-pressure cooling of protein crystals without cryoprotectants. *Acta Crystallogr D* 61:881–890.
24. Kim CU, Hao Q, Gruner SM (2006) Solution of protein crystallographic structures by high-pressure cryocooling and noble-gas phasing. *Acta Crystallogr D* 62:687–694.
25. Kim CU, Hao Q, Gruner SM (2007) High-pressure cryocooling for capillary sample cryoprotection and diffraction phasing at long wavelengths. *Acta Crystallogr D* 63:653–659.
26. Barstow B, Ando N, Kim CU, Gruner SM (2008) Alteration of citrine structure by hydrostatic pressure explains the accompanying spectral shift. *Proc Natl Acad Sci USA* 105:13362–13366.
27. Kim CU, Chen Y-F, Tate MW, Gruner SM (2008) Pressure induced high-density amorphous ice in protein crystals. *J Appl Crystallogr* 41:1–7.
28. Ravelli RBG, Theveneau P, McSweeney S, Caffrey M (2002) Unit-cell volume change as a metric of radiation damage in crystals of macromolecules. *J Synchrotron Radiat* 9:355–360.
29. Harp JM, Timm DE, Bunick GJ (1998) Macromolecular crystal annealing: Overcoming increased mosaicity associated with cryocrystallography. *Acta Crystallogr D* 54:622–628.
30. Yeh JI, Hol WG (1998) A flash-annealing technique to improve diffraction limits and lower mosaicity in crystals of glycerol kinase. *Acta Crystallogr D* 54:479–480.
31. Weik M, et al. (2005) Supercooled liquid-like solvent in trypsin crystals: Implications for crystal annealing and temperature-controlled X-ray radiation damage studies. *J Synchrotron Radiat* 12:310–317.
32. Ringe D, Petsko GA (1986) Study of protein dynamics by X-ray diffraction. *Methods Enzymol* 131:389–433.
33. Malkin AJ, Thorne RE (2004) Growth and disorder of macromolecular crystals: Insights from atomic force microscopy and X-ray diffraction studies. *Methods* 34:273–299.
34. Smith RS, Kay BD (1999) The existence of supercooled liquid water at 150 K. *Nature* 398:788–791.
35. Weik M, Lehnert U, Zaccai G (2005) Liquid-like water confined in stacks of biological membranes at 200 K and its relation to protein dynamics. *Biophys J* 89:3639–3646.
36. Mallamace F, et al. (2007) Evidence of the existence of the low-density liquid phase in supercooled, confined water. *Proc Natl Acad Sci USA* 104:424–428.
37. Bhattacharyya K (2008) Nature of biological water: A femtosecond study. *Chem Commun* 2848–2857.
38. Chen S-H, et al. (2006) The violation of the Stokes–Einstein relation in supercooled water. *Proc Natl Acad Sci USA* 103:12974–12978.
39. Chen S-H, et al. (2006) Observation of fragile-to-strong dynamic cross-over in protein hydration water. *Proc Natl Acad Sci USA* 103:9012–9016.
40. Rossman MG, van Beek CG (1999) Data processing. *Acta Crystallogr D* 55:1631–1640.
41. Otwinowski Z, Minor W (1997) Processing of X-ray diffraction data collected in oscillation mode. *Methods Enzymol* 276:307–326.
42. Vagin A, Teplyakov A (1997) *MOLREP*: An automated program for molecular replacement. *J Appl Crystallogr* 30:1022–1025.
43. Collaborative Computational Project No. 4 (1994) The CCP4 suite: Programs for protein crystallography. *Acta Crystallogr D* 50:760–763.
44. Murshudov GN, Vagin A, Dodson EJ (1997) Refinement of macromolecular structures by the maximum-likelihood method. *Acta Crystallogr D* 53:240–255.
45. Emsley P, Cowtan K (2004) Coot: Model-building tools for molecular graphics. *Acta Crystallogr D* 60:2126–2132.
46. DeLano W (2002) PyMol (DeLano Scientific, Palo Alto, CA).

Supporting Information

Kim et al. 10.1073/pnas.0812481106

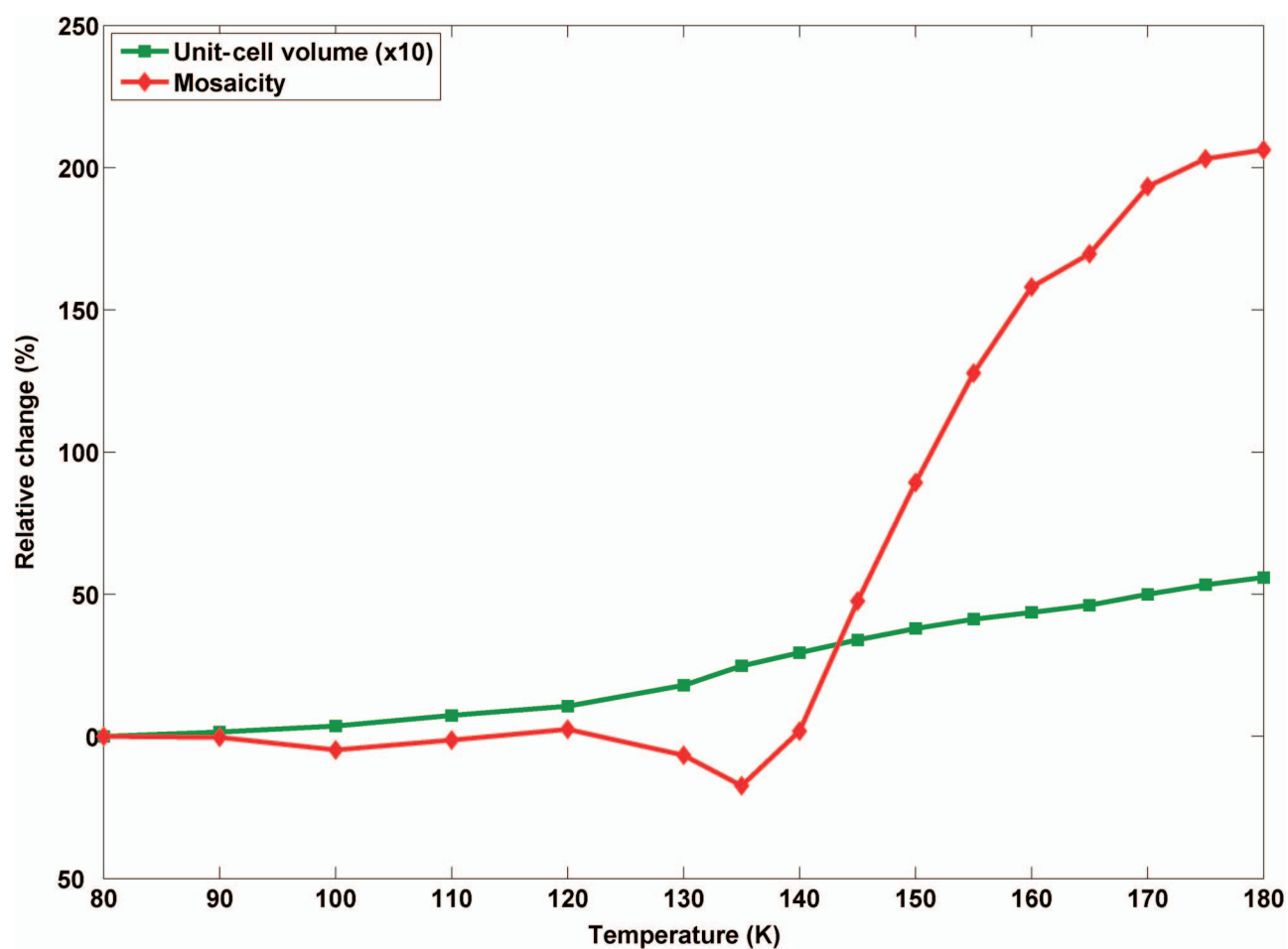**Fig. S1.** Thaumatin high-pressure cryocooled at 200 MPa. Results from complete data sets were used to generate the unit-cell volume and mosaicity profiles. Mosaicity and unit-cell volume were computed with HKL2000.
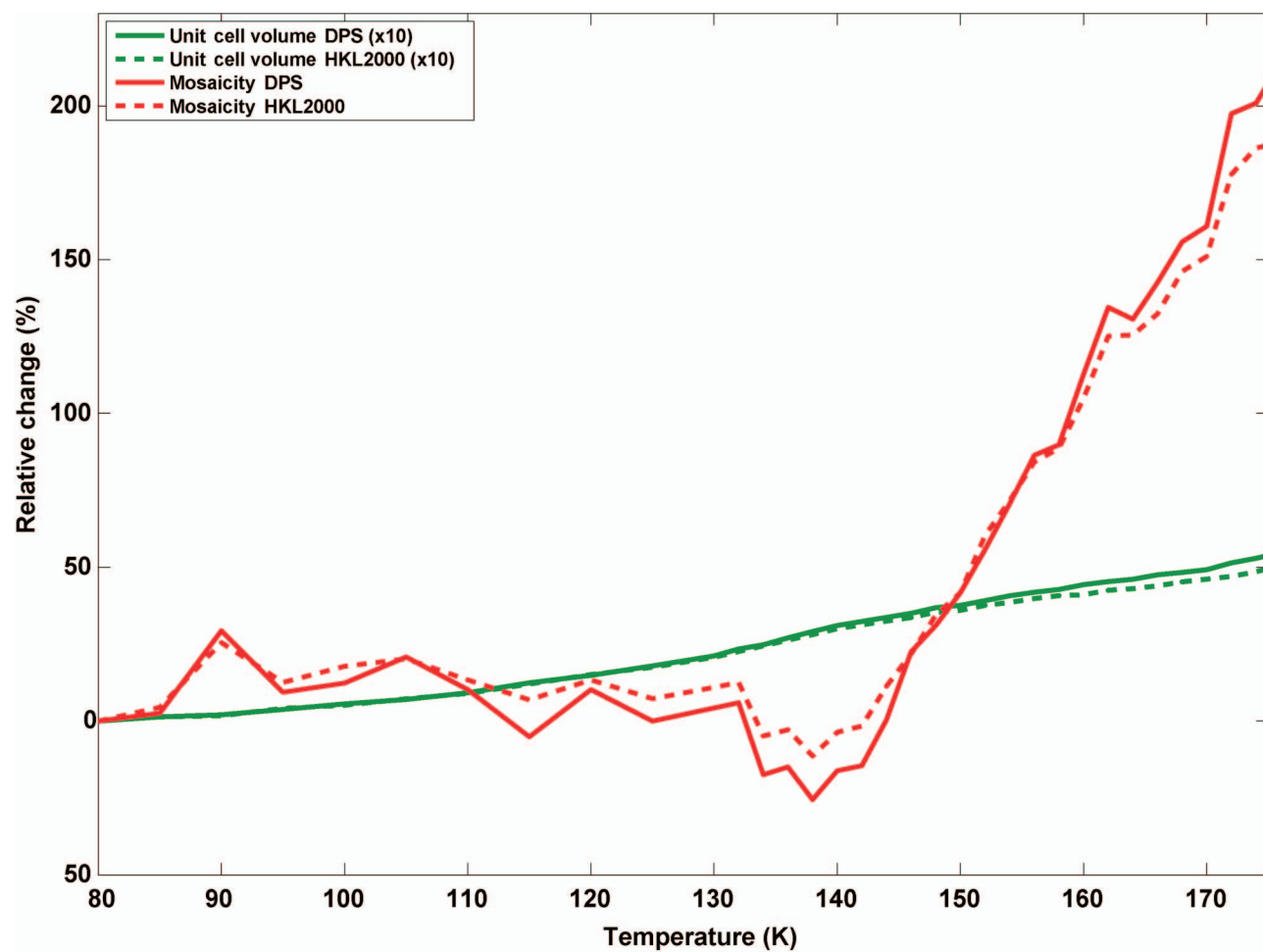
Fig. S2. Comparison of calculations by DPS and HKL2000 of unit-cell volume and mosaicity of thaumatin high-pressure cryocooled at 200 MPa. Note that both programs produce the same trends as temperature is raised.

Table S1. Data collection statistics for the thaumatin high-pressure cryocooled at 200 MPa

K	Unit-cell dimensions, Å		Resolution, Å	Mosaicity, °	R_{sym}*	$I/\sigma(I)$	Completeness, %	Redundancy
	a = b	c						
80	57.43	149.900	30–1.9 (1.97–1.9)	0.317	0.029	49.2 (19.4)	98.4 (87.0)	4.4 (3.1)
90	57.46	149.975	30–1.9 (1.97–1.9)	0.316	0.041	35.1 (14.0)	98.3 (86.6)	4.4 (3.1)
100	57.50	150.002	30–1.9 (1.97–1.9)	0.302	0.034	39.9 (16.6)	98.3 (86.7)	4.3 (3.1)
110	57.60	150.080	30–1.9 (1.97–1.9)	0.313	0.030	48.3 (18.4)	98.2 (86.2)	4.4 (3.1)
120	57.66	150.255	30–1.9 (1.97–1.9)	0.325	0.029	48.2 (18.1)	98.3 (86.8)	4.4 (3.1)
130	57.82	150.530	30–1.9 (1.97–1.9)	0.296	0.028	49.4 (19.2)	98.2 (86.2)	4.4 (3.1)
135	57.97	150.747	30–1.9 (1.97–1.9)	0.262	0.026	53.1 (22.9)	98.1 (85.7)	4.4 (3.1)
140	58.08	150.878	30–1.9 (1.97–1.9)	0.323	0.027	50.5 (21.0)	98.1 (85.8)	4.4 (3.1)
145	58.19	150.967	30–1.9 (1.97–1.9)	0.468	0.027	50.2 (18.7)	97.9 (84.7)	4.4 (3.7)
150	58.29	151.017	30–1.9 (1.97–1.9)	0.600	0.030	45.6 (14.6)	98.0 (85.4)	4.4 (3.1)
155	58.38	151.026	30–1.9 (1.97–1.9)	0.722	0.037	37.8 (10.1)	98.0 (85.7)	4.4 (3.1)
160	58.45	150.996	30–1.9 (1.97–1.9)	0.818	0.046	31.0 (7.3)	98.0 (86.2)	4.4 (3.1)
165	58.53	150.986	30–1.9 (1.97–1.9)	0.855	0.052	28.7 (5.7)	98.0 (86.4)	4.4 (3.0)

The space group is P4$_1$2$_1$2 in all cases. Values in parentheses are for the highest-resolution shell. Statistics were calculated with HKL2000.
*$R_{sym} = \Sigma |I - \langle I \rangle| / \Sigma \langle I \rangle$.

Table S2. Data collection statistics for thaumatin cryocooled at ambient pressure and thaumatin at ambient conditions (0.1 MPa and 293 K)

K	Unit-cell dimensions, Å		Resolution, Å	Mosaicity,°	R_{sym}*	$I/\sigma(I)$	Completeness, %	Redundancy
	a = b	c						
Cryocooled at ambient pressure								
80	57.760	149.803	30–1.9 (1.97–1.9)	0.377	0.043	30.9 (13.2)	97.0 (92.8)	4.4 (2.8)
90	57.776	149.841	30–1.9 (1.97–1.9)	0.378	0.057	24.8 (11.0)	97.1 (93.2)	4.4 (2.9)
100	57.786	149.876	30–1.9 (1.97–1.9)	0.376	0.044	29.8 (12.8)	97.2 (93.1)	4.5 (2.9)
110	57.798	149.915	30–1.9 (1.97–1.9)	0.376	0.043	30.0 (12.9)	97.3 (93.5)	4.5 (2.9)
120	57.811	149.958	30–1.9 (1.97–1.9)	0.374	0.041	31.0 (13.2)	97.3 (93.4)	4.4 (2.9)
130	57.824	149.997	30–1.9 (1.97–1.9)	0.373	0.041	30.9 (13.0)	97.3 (93.4)	4.4 (2.9)
135	57.831	150.018	30–1.9 (1.97–1.9)	0.375	0.041	30.9 (12.9)	97.3 (93.3)	4.4 (2.9)
140	57.842	150.045	30–1.9 (1.97–1.9)	0.375	0.043	30.3 (12.2)	97.3 (93.1)	4.4 (2.8)
145	57.854	150.075	30–1.9 (1.97–1.9)	0.376	0.042	31.1 (12.6)	97.4 (93.5)	4.4 (2.9)
150	57.867	150.106	30–1.9 (1.97–1.9)	0.378	0.042	30.8 (12.4)	97.4 (93.4)	4.4 (2.9)
155	57.886	150.144	30–1.9 (1.97–1.9)	0.380	0.042	30.8 (12.0)	97.4 (93.6)	4.4 (2.9)
160	57.914	150.191	30–1.9 (1.97–1.9)	0.379	0.042	30.8 (12.0)	97.4 (93.5)	4.4 (2.9)
165	57.962	150.258	30–1.9 (1.97–1.9)	0.382	0.042	31.0 (11.9)	97.4 (93.7)	4.4 (2.9)
At ambient conditions (0.1 MPa, 293 K)								
293	58.565	151.483	30–.19 (1.97–1.9)	0.099	0.0700	20.6 (4.7)	99.9 (99.9)	4.2 (2.6)

The space group is $P4_12_12$ in all cases. Values in parentheses are for the highest resolution shell. Statistics were calculated with HKL2000.

*$R_{sym} = \Sigma |I - \langle I \rangle| / \Sigma \langle I \rangle$.

Table S3. Refinement statistics of thaumatin

K	Unique reflections	R factor*	R_{free} factor†	No. water molecules	B factors, Å²	
					Protein (main/side)	Water
High-pressure cryocooled at 200 MPa						
80	20,343	0.159	0.200	429	9.19/10.52	25.66
90	20,347	0.161	0.203	416	9.47/10.90	25.35
100	20,390	0.161	0.207	417	9.69/11.12	25.61
110	20,455	0.161	0.216	415	10.12/11.55	26.05
120	20,505	0.159	0.214	418	10.25/11.67	26.62
130	20,646	0.159	0.204	418	10.22/11.76	26.86
135	20,767	0.160	0.212	413	10.09/11.63	26.82
140	20,843	0.160	0.207	415	10.67/12.21	27.92
145	20,922	0.160	0.200	427	11.86/13.45	30.12
150	21,003	0.163	0.217	388	13.43/15.02	30.21
155	21,088	0.167	0.212	385	14.98/16.52	32.30
160	21,150	0.170	0.210	357	16.78/18.30	33.53
165	21,219	0.172	0.210	315	18.31/19.94	32.91
Cryocooled at ambient pressure						
80	20,434	0.150	0.191	404	10.29/11.72	28.95
90	20,231	0.152	0.194	390	10.50/12.07	28.24
100	20,249	0.150	0.191	402	10.52/11.99	29.38
110	20,232	0.149	0.188	409	10.67/12.15	29.99
120	20,310	0.150	0.199	404	10.72/12.21	29.74
130	20,331	0.152	0.180	390	10.83/12.37	29.38
135	20,334	0.150	0.185	399	10.91/12.44	29.62
140	20,549	0.149	0.191	407	11.03/12.61	30.76
145	20,363	0.151	0.185	399	11.12/12.69	30.00
150	20,384	0.153	0.186	396	11.20/12.81	30.10
155	20,394	0.152	0.186	388	11.39/12.98	30.19
160	20,432	0.153	0.195	392	11.47/13.11	30.21
165	20,493	0.152	0.194	383	11.77/13.42	30.70
At ambient conditions (0.1 MPa, 293 K)						
293	21,653	0.159	0.184	202	17.61/20.16	38.48

*R factor = Σ |F_o| − |F_c|/Σ |F_{obs}|.
†R_{free} factor is calculated the same as R factor, except it uses 5% of reflection data omitted from refinement.